

Supplement material

1.1 FIGAERO-CIMS declustering

As described in section 2.2, we observed a considerable amount of declustered ions in the FIGAERO-CIMS mass spectra. We speculate that a possible declustering process was the removal of HI from $[M+I]^-$ adducts, leaving behind $[M-H]^-$ to be detected, e.g., carboxylate anions following the deprotonation of the corresponding carboxylic acids. However, it is also possible that other decomposition reactions occurred, such as decomposition of peroxyacid-iodide adducts into carboxylate anions ($[M-OH]^-$; Lee et al., 2014), decarboxylation $[M-H-CO_2]^-$ and/or dehydration of carboxylic acids and alcohols $[M-H-H_2O]^-$ (e.g. Canagaratna et al., 2015; Stark et al., 2017), or cleavage of weak organic peroxide bonds (Iyer et al., 2016; Schobesberger et al., 2018). In general, declustered ions were observed at relatively lower average desorption temperatures. Either the respective parent compounds are, on average, more volatile than compounds observed as $[M+I]^-$, or higher desorption temperatures induce decomposition processes that forestall potential CIMS-induced decomposition. Clearly, dedicated studies are warranted to gain a mechanistic understanding of the combination of thermally induced (in the FIGAERO) and collision-induced (in the CIMS) dissociation of ion clusters and/or molecules.

1.2 FIGAERO-CIMS average values

For the FIGAERO data, the average composition and elemental ratios were derived from the identified molecular formula for each ion. The average composition (average number of C, H, and O atoms) was calculated as the signal weighted sum:

$$composition = \sum_i (C_i \cdot f_i), \sum_i (H_i \cdot f_i), \sum_i (O_i \cdot f_i) \quad (S1)$$

With C_i , H_i , and O_i being the number of C, H, and O atoms in the molecular formula for each ion i and f_i the normalised signal of the ion i , i.e., the count rate of ion i normalising to the sum over all non-reagent ions.

For each identified molecular formula, the O:C and H:C ratios were calculated. The average O:C and H:C ratios were calculated as the signal weighted sum of these:

$$\overline{O:C} = \sum_i ((O:C)_i \cdot f_i) \quad (S2)$$

$$\overline{H:C} = \sum_i ((H:C)_i \cdot f_i) \quad (S3)$$

with $(O:C)_i$ (or $(H:C)_i$) being the O:C (or H:C) ratio calculated from the molecular formula of each ion i and f_i the normalised signal of the ion i . Note that this is not the same as the ratio of O and C in the average composition.

1.3 Modelling of evaporation

The evaporation inside the RTC was modelled with two different process models. The models were used together with an optimization algorithm to investigate if the difference in evaporation between 80% and 40% RH can be explained by the

solution effect (Raoult's law). In both models the particle composition was presented with a one-dimensional VBS (Donahue et al., 2006) with 6 compounds or 'bins' spanning from $10^{-3} \mu\text{g m}^{-3}$ to $10^2 \mu\text{g m}^{-3}$ with a decade difference between two adjacent bins. The evaporation at RH40% and RH80% was modelled with a liquid-like evaporation model (LLEVAP; Yli-Juuti et al. (2017)) where the particles are assumed to behave like well-mixed liquids. Thus, the limiting step in evaporation is the transport of mass between particle and gas phases. The evaporation under dry conditions was modelled with a slightly modified version of the kinetic multi-layer model for gas-particle interactions in aerosols and clouds (KM-GAP, Shiraiwa et al., 2012; Yli-Juuti et al., 2017). In KM-GAP, the viscosity in each layer of the particle was expressed with a mixing rule (O'Meara et al., 2016):

$$\log_{10}(\eta_j) = \sum_{i=1}^N X_{mole,i,j} \log_{10}(b_i) \quad (S4)$$

where η_j is the viscosity in the j th layer, $X_{mole,i,j}$ is the molar fraction of the i th compound in j th layer, and b_i is a coefficient that describes to which extent compound i affects the viscosity. The particle phase diffusion coefficients were calculated from the viscosity with the Stokes-Einstein equation. Both models assume ideal solution and calculate the water uptake based on continuous equilibrium between gas and particle phase (Yli-Juuti et al., 2017). In all simulation cases, the molar masses of each bin were set to 200 g mol^{-1} , particle phase densities to 1200 kg m^{-3} , and gas phase diffusion coefficients to $0.05 \text{ cm}^2 \text{ s}^{-1}$.

The two process models were coupled to a global optimization algorithm Monte Carlo Genetic Algorithm (MCGA, Berkemeier et al., 2017). In the optimization process, the free parameters, i.e. the parameters that the MCGA can vary, were the mole fraction of each VBS bin when the particles enter the residence time chamber and the coefficients b_i in Eq. S4. The MCGA was set to seek for a set of free parameters that minimizes the mean-squared-error between the measured and simulated evapograms. For each OC case, the parameters were optimized simultaneously to evaporation data at RH80% and dry conditions. This yields the initial particle composition in term of the VBS bins assuming that the difference between evaporation rates is controlled by the low particle phase diffusivity in dry conditions. This initial composition is expected to be the same for all humidity conditions due to the experimental procedure. The initial composition was then used in the LLEVAP to simulate evaporation at RH40%.

The resulting evapogram curves are shown in Figure S4 for all experiments.

1.4 SI References

Berkemeier, T., Ammann, M., Krieger, U. K., Peter, T., Spichtinger, P., Pöschl, U., Shiraiwa, M. and Huisman, A. J.: Technical note: Monte Carlo genetic algorithm (MCGA) for model analysis of multiphase chemical kinetics to determine transport and reaction rate coefficients using multiple experimental data sets, *Atmos. Chem. Phys.*, 17(12), 8021–8029, doi:10.5194/acp-17-8021-2017, 2017.

Canagaratna, M. R., Jimenez, J. L., Kroll, J. H., Chen, Q., Kessler, S. H., Massoli, P., Hildebrandt Ruiz, L., Fortner, E., Williams, L. R., Wilson, K. R., Surratt, J. D., Donahue, N. M., Jayne, J. T. and Worsnop, D. R.: Elemental ratio measurements of organic compounds using aerosol mass spectrometry: Characterization, improved calibration, and implications, *Atmos. Chem. Phys.*, 15(1), 253–272, doi:10.5194/acp-15-253-2015, 2015.

Iyer, S., Lopez-Hilfiker, F., Lee, B. H., Thornton, J. A. and Kurtén, T.: Modeling the Detection of Organic and Inorganic Compounds Using Iodide-Based Chemical Ionization, *J. Phys. Chem. A*, 120(4), 576–587, doi:10.1021/acs.jpca.5b09837,

2016.

Lee, B. H., Lopez-Hilfiker, F. D., Mohr, C., Kurtén, T., Worsnop, D. R. and Thornton, J. A.: An iodide-adduct high-resolution time-of-flight chemical-ionization mass spectrometer: Application to atmospheric inorganic and organic compounds, *Environ. Sci. Technol.*, 48(11), 6309–6317, doi:10.1021/es500362a, 2014.

- 5 O’Meara, S., Topping, D. O. and McFiggans, G.: The rate of equilibration of viscous aerosol particles, *Atmos. Chem. Phys.*, 16(8), 5299–5313, doi:10.5194/acp-16-5299-2016, 2016.

Schobesberger, S., D’Ambro, E. L., Lopez-Hilfiker, F. D., Mohr, C. and Thornton, J. A.: A model framework to retrieve thermodynamic and kinetic properties of organic aerosol from composition-resolved thermal desorption measurements, *Atmos. Chem. Phys. Discuss.*, 1–50, doi:10.5194/acp-2018-398, 2018.

- 10 Shiraiwa, M., Pfrang, C., Koop, T. and Pöschl, U.: Kinetic multi-layer model of gas-particle interactions in aerosols and clouds (KM-GAP): linking condensation, evaporation and chemical reactions of organics, oxidants and water, *Atmos. Chem. Phys.*, 12(5), 2777–2794, doi:10.5194/acp-12-2777-2012, 2012.

Stark, H., Yatavelli, R. L. N., Thompson, S. L., Kang, H., Krechmer, J. E., Kimmel, J. R., Palm, B. B., Hu, W., Hayes, P. L., Day, D. A., Campuzano-Jost, P., Canagaratna, M. R., Jayne, J. T., Worsnop, D. R. and Jimenez, J. L.: Impact of Thermal Decomposition on Thermal Desorption Instruments: Advantage of Thermogram Analysis for Quantifying Volatility Distributions of Organic Species, *Environ. Sci. Technol.*, 51(15), 8491–8500, doi:10.1021/acs.est.7b00160, 2017.

- 15

Yli-Juuti, T., Pajunoja, A., Tikkanen, O. P., Buchholz, A., Faiola, C., Väisänen, O., Hao, L., Kari, E., Peräkylä, O., Garmash, O., Shiraiwa, M., Ehn, M., Lehtinen, K. and Virtanen, A.: Factors controlling the evaporation of secondary organic aerosol from a-pinene ozonolysis, *Geophys. Res. Lett.*, 44(5), 2562–2570, doi:10.1002/2016GL072364, 2017.

20 1.5 SI Tables

Table S1: Parameters in the PAM for different experiment settings.

	low	medium	high
T / °C	27	27	27
RH / %	40	40	40
[VOC] / ppb	190	190	190
[O₃]_{inlet} / ppb	6.6	25	25
[O₃]_{outlet} / ppb	6.4	22.2	16
OH exposure / cm⁻³ s	2.54e11	6.85e11	2.45e12
photochemical age / days	1.96	5.3	18.9

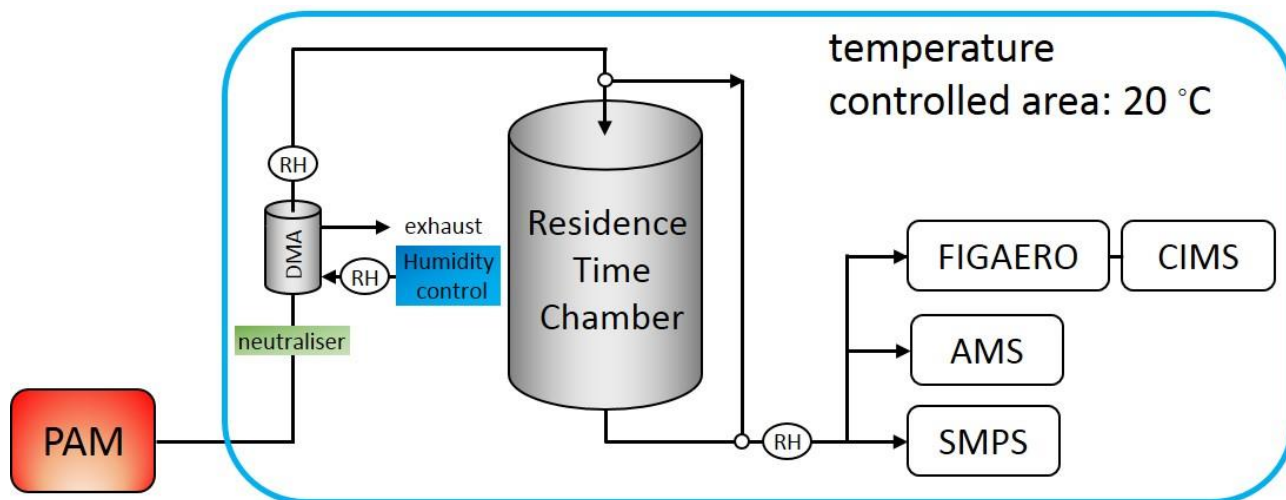
Table S2: FIGAERO sampling and desorption parameters.

	fresh	RTC
sampling time / min	20 or 30	20
sampling flow / lpm	2	10
collected mass / ng	140 – 300	20 – 70
desorption time / min	ramp: 15 soak at 200 C: 15	ramp: 15 soak at 200 C: 15
temperature ramp / °C/min	12	12

Table S3: Estimated collected sample mass on FIGAERO filter

OH exposure	condition	sample mass / ng	
		fresh	RTC
low	dry	178	33
	RH80%	186	22
medium	dry	239	72
	RH80%	258	50
high	dry	138	46
	RH80%	172	30

1.6 SI Figures



5 Figure S1: Schematic diagram of the experimental setup used for measuring the rate and extent of evaporation from SOA particles.

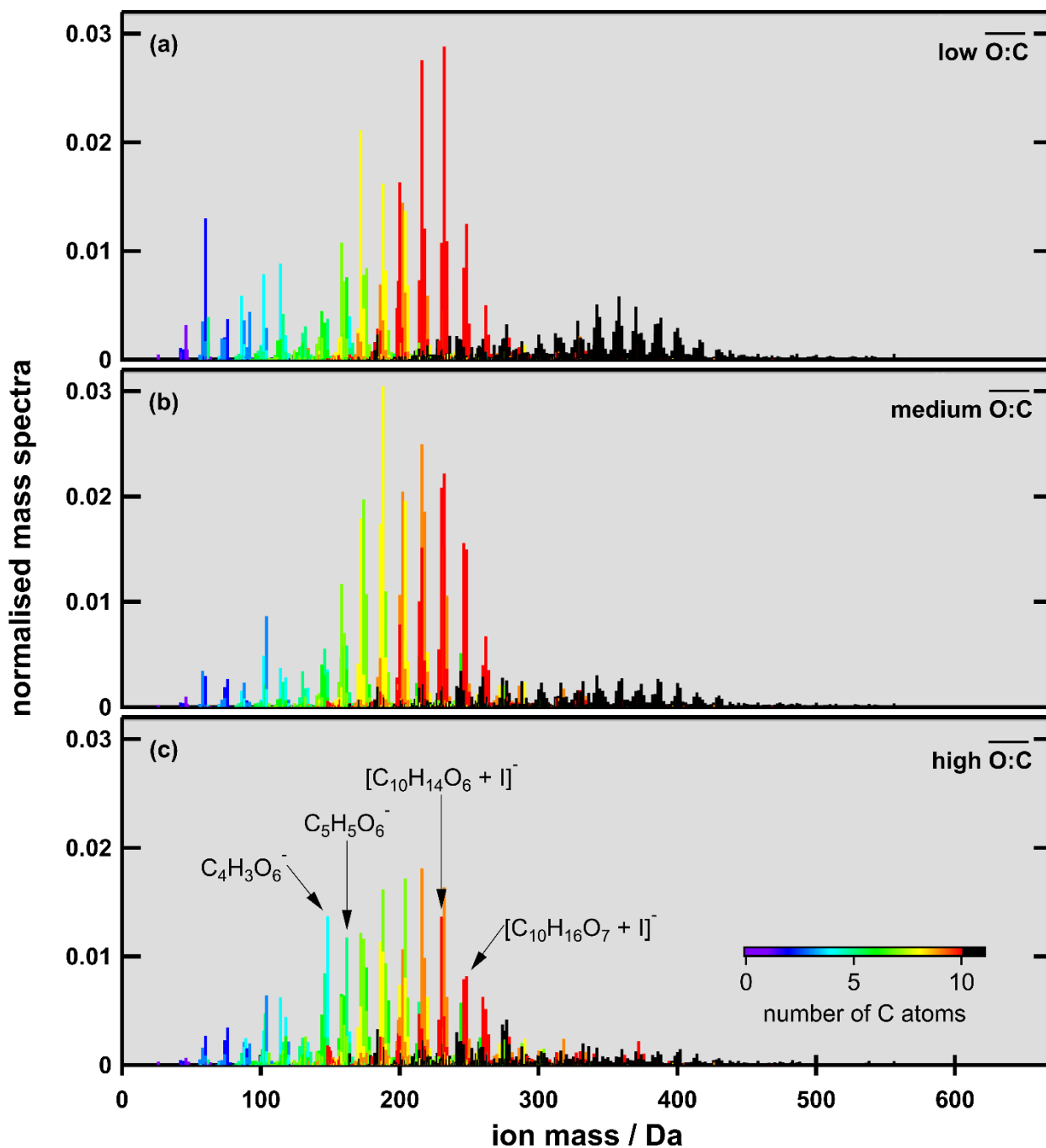


Figure S2: Normalised integrated mass spectra for fresh, dry SOA from low-, medium- and high-O:C cases. Signal is normalised to total signal and colour-coded with the number of C atoms per molecule. Black indicates 11 or more C atoms, which means that these ions stem from the combination of at least two organic molecules (dimers). The contribution of the clustered iodide ions is removed from the plotted ion mass. The ions $C_4H_3O_6^-$, $C_5H_5O_6^-$, $[C_{10}H_{14}O_6 + I]^-$, and $[C_{10}H_{16}O_7 + I]^-$, which are analysed in more detail in section 3.3 in the main text, are marked for the high-O:C case.

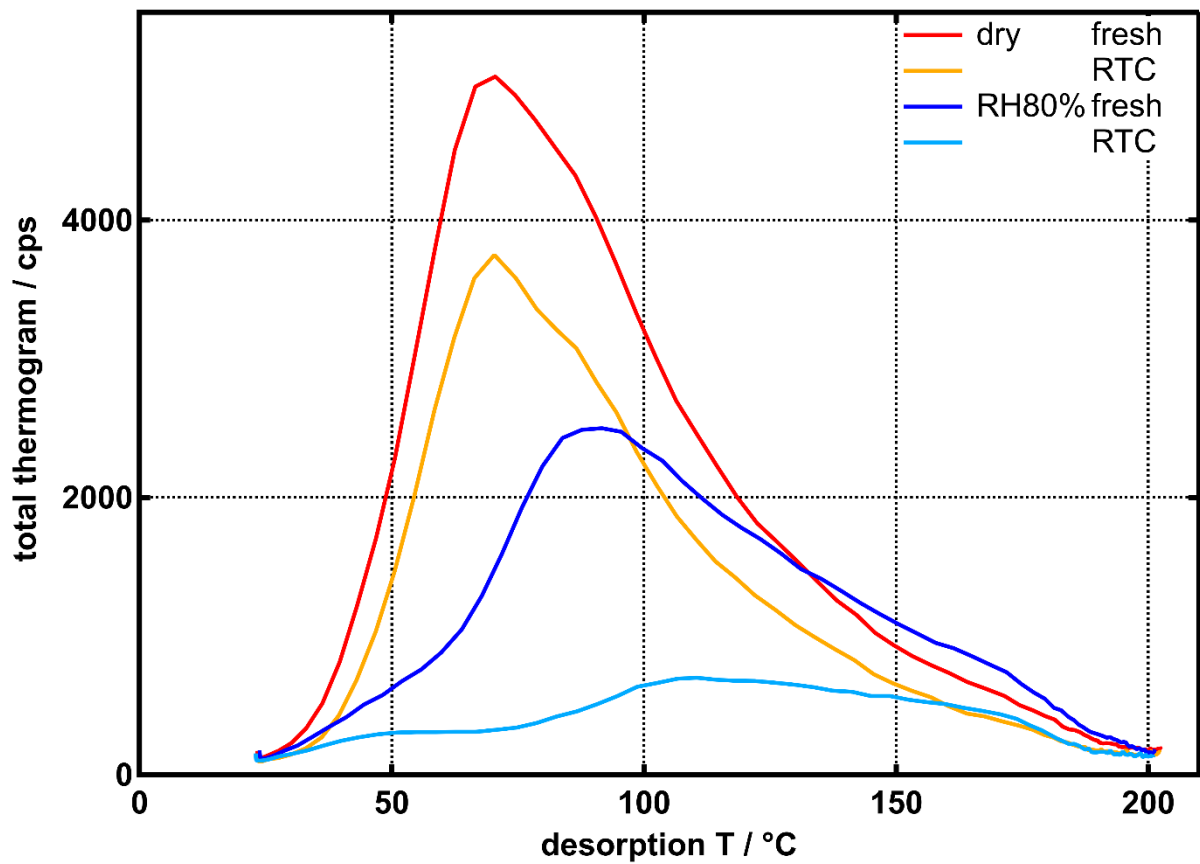


Figure S3: Non-normalised thermograms for the high- O_3 case. RTC refers to particles stored in the RTC for 3 - 4 h before being analysed by FIGAERO-CIMS.

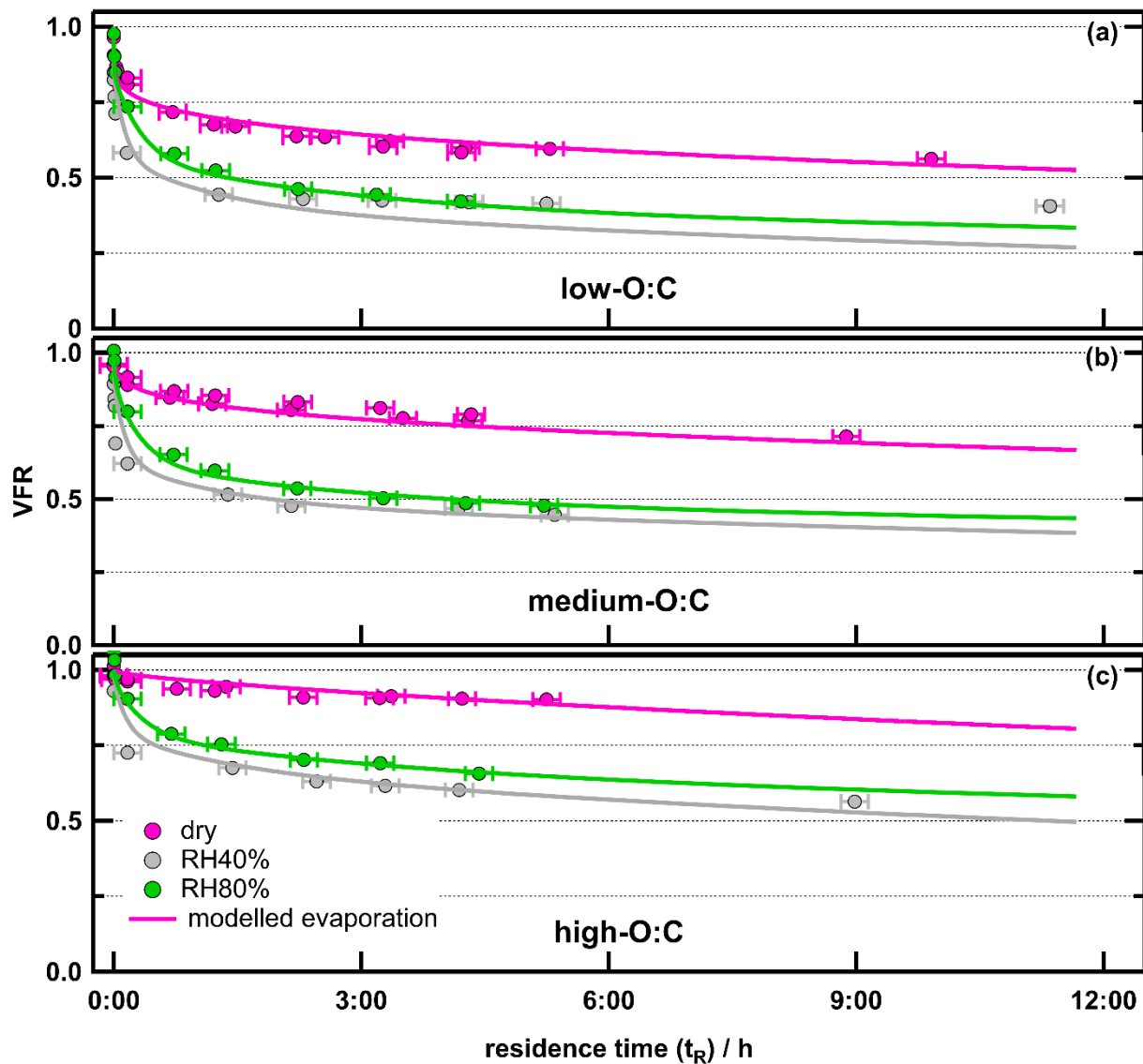


Figure S4: Measured (circles) and modelled (lines) evapograms for all experiment cases.

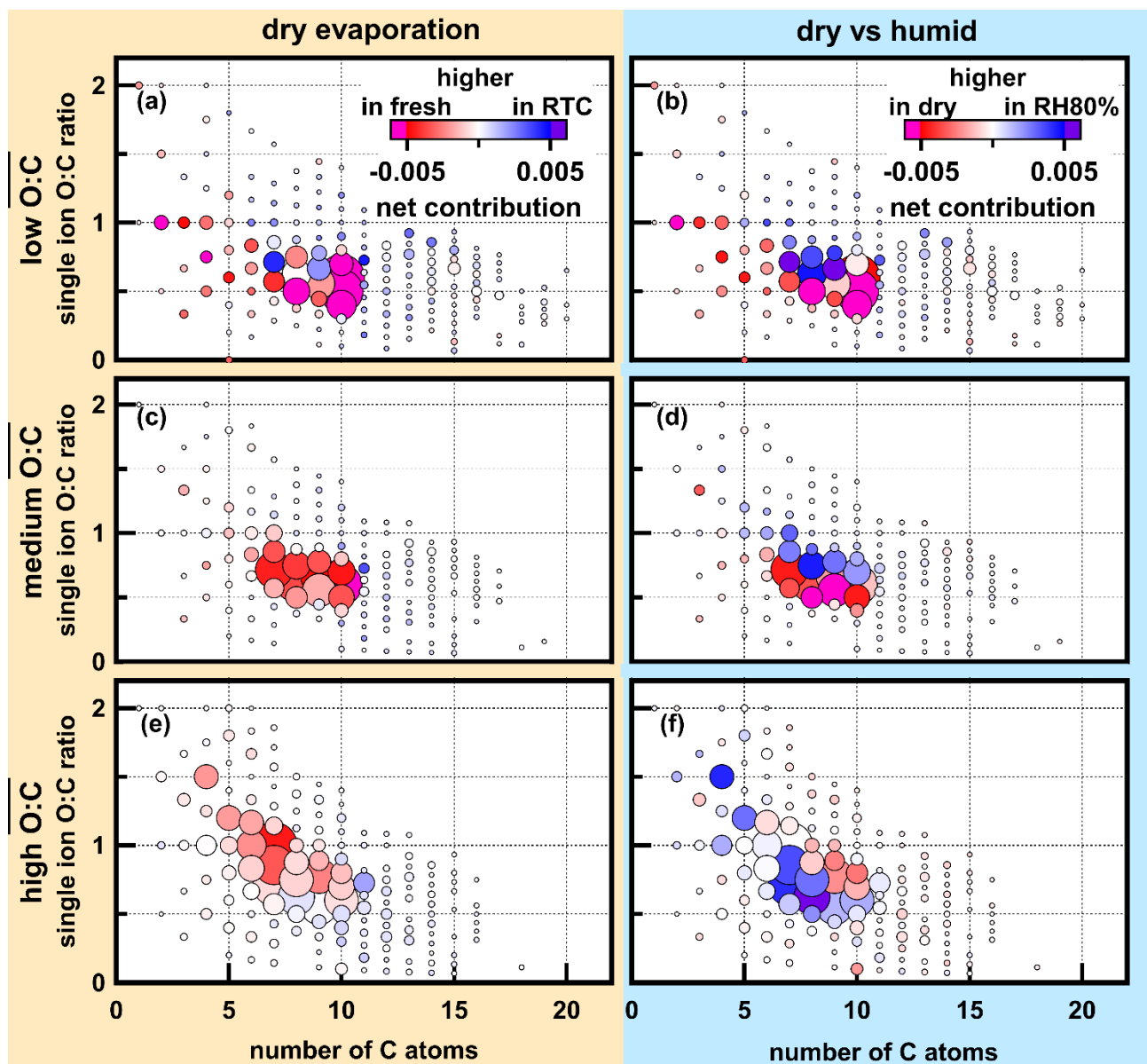


Figure S5: Individual O:C ratios of the detected molecules in normalised integrated mass spectra for dry, fresh SOA particles in low-, medium- and high-O:C cases. All ions with the same O:C ratio for a given carbon chain length were added up. Symbol size indicates signal strength for the dry, fresh SOA case, and colour code illustrates the changes due to isothermal evaporation under dry conditions (panels (a), (c), and (e)) and between fresh SOA under dry and RH80% conditions (panels (b), (d), and (f)). Red colours indicate higher contributions in the fresh, dry case while blue colours indicate a net increase with evaporation or humidification.

5